

Superradiant instability of area-quantized Kerr black hole with discrete reflectivity

Zhong-Hao Luo^{1,3,4*} and Yun-Long Zhang^{2,1,5†}

¹*School of Fundamental Physics and Mathematical Sciences,*

Hangzhou Institute for Advanced Study, UCAS, Hangzhou 310024, China.

²*National Astronomy Observatories, Chinese Academy of Science, Beijing, 100101, China*

³*CAS Key Laboratory of Theoretical Physics, Institute of Theoretical Physics,*

Chinese Academy of Sciences, Beijing 100190, China.

⁴*University of Chinese Academy of Sciences, Beijing 100149, China. and*

⁵*International Center for Theoretical Physics Asia-Pacific, Beijing/Hangzhou, China*

(Dated: August 13, 2024)

Ultralight bosons can condense to form the so-called bosonic clouds around rotating black holes by superradiance instability. When quantum effects are taken into account, the classical black hole is replaced by an exotic compact object including an area-quantized black hole. In this work, we consider the superradiant instability of massive scalar fields around area-quantized Kerr black holes. Firstly, we get the transition spectral lines of area-quantized black holes for scalar fields by the angular momentum conservation of the scalar field and the black hole. Subsequently, we compute the growth rate of scalar clouds around exotic compact objects. We introduce the reflectivity of area-quantized black holes for massive scalar fields. Then we consider the case of the scalar fields that can be superradiated by area-quantized black holes. Finally, we found the area quantization of black holes can affect the formation, mass, and location of the scalar clouds.

Contents

I. Introduction	2
II. Area-quantized black hole	3
A. The discrete energy spectrum	4
B. Transition spectral lines and line width	5
III. Superradiant instability of scalar field	6

*Electronic address: luozhonghao22@mailsucas.ac.cn

†Electronic address: zhangyunlong@nao.cas.cn

A. Growth rate of superradiant instability	6
B. Reflectivity with discrete feature	8
IV. Scalar cloud around area-quantized black hole	10
A. Suppression and mass of scalar cloud	11
B. Bohr radius of scalar cloud	14
V. Conclusion	15
Acknowledgments	16
A. The absorption approximate formula	16
B. Solving the radial equation	17
1. The far region solution	17
2. The near region solution	18
3. The overlap region solution	22
References	23

I. INTRODUCTION

Ultralight bosons are one of the most well-motivated classes of particles proposed as potential candidates for dark matter, interacting weakly with ordinary matter [1–6]. For their extreme small masses, especially when the corresponding Compton wavelength of ultralight bosons is about to or larger than the order of black hole scale, the ultralight bosons can be spontaneously amplified to extract the energy and angular momenta of rotating black holes to generate an exponentially growing bosonic cloud. The mechanism is known as superradiant instability [7–12]. This system, so-called gravitational atom [7, 13, 14], is considered to an important gravitational wave source and can be used to constrain parameters of ultralight bosons [15–24].

To resolve the information-loss paradox [25, 26], alternatives to classical black hole have been proposed to take into account quantum modifications of the gravity theory near Planck scale of event horizon, like a gravastar [27], boson star [28], and fullball [29]. They are commonly known as exotic compact objects (ECOs). For classical black holes, due to the causal structure of the geometry, their null surface is a one-way membrane. So classical black holes are perfect

absorbers namely possessing zero reflectivity. But unlike classical black holes, ECOs possess non-zero reflectivity to result from a surface reflecting the fields outwards. An interesting one of ECOs, an area-quantized black hole with a discrete mass spectrum, absorbs energy only at the selected frequencies. Then the area-quantized black holes can only undergo transition to discrete energy levels [30].

An area-quantized black hole is a phenomenological model proposed by Bekenstein and Mukhanov [31], and has been constructed from the first principle approach in loop quantum gravity [32–38]. Any such modification of the boundary condition at the event horizon from non-zero reflectivity is expected to affect the response of black hole to external perturbation [39, 40]. The superradiant instability phenomenon is essentially a boundary value problem from a mathematical point of view. So the reflectivity of the modified models to black holes is manifested as different superradiant instability phenomenons.

In this paper, we investigate the superradiant instability of massive scalar fields around area-quantized black holes. We use the non-relativistic approximation to solve the Klein-Gordon equation. We obtain the analytical expression for the growth rate of scalar clouds in the case of exotic compact objects. Then, we model the reflectivity of area-quantized black holes, which can reflect the selected property of the area-quantized black holes. As a result, we show the influences on the scalar clouds due to the area quantization.

This paper is organized as follows. In Section II, we briefly review the unique discrete property of area-quantized black holes. We reveal the absorption/transition spectral lines of area-quantized black holes absorbing scalar fields. In Section III, we first compute the growth rate of scalar clouds around exotic compact objects. Then we model the reflectivity of area-quantized black holes for scalar fields, which corresponds to the absorption situation. In Section IV, we consider the absorption of the scalar fields that meet the superradiance condition. Then, we study the effects of scalar clouds from the area quantization of black holes. In Section V, we conclude with a discussion and outlook of the results. In this work, we use the $(-, +, +, +)$ convention and take the unit $G = c = 1$.

II. AREA-QUANTIZED BLACK HOLE

Area quantization of black holes has been introduced by Bekenstein in his pioneering work [41]. Though Christodoulou’s work [42], Hawking’s area invariance theory [43], it was included that the horizon region of a non-extreme black hole can be regarded as a classical adiabatic invariant.

According to Ehrenfest's principle, any classical adiabatic invariant corresponds to a quantum entity with a discrete spectrum. In Christodoulous's work [42], it can be regarded as an adiabatic process when an uncharged particle undergoes the event horizon of a black hole at its own radial turning point. The area of this black hole remains invariant, as well as the changes of other eliminated parameters.

A. The discrete energy spectrum

In [41], considering Heisenberg's uncertainty principle in the quantum theory, Bekenstein suggests that a classical point particle turns into a particle with an inherent radius. So, the area change of the black hole is not zero but a finite value, namely $\Delta A_{\min} = 8\pi\mu b_\mu$, where μ is the mass of this particle, and b_μ is the inherent radius of this particle. If $b_\mu = 0$, then it recovers the classical situation. However, a relativistic particle can not be localized within the Compton wavelength. The finite radius of this particle meets $b_\mu \geq \lambda_\mu \equiv \hbar/\mu$. So the minimum area change of a black hole in the quantum theory is $\Delta A_{\min} = 8\pi\ell_P^2$, where $\ell_P = \sqrt{\hbar G/c^3}$ is Planck scale.

When the particle carries an electric charge, the minimum area change is $\Delta A_{\min} = 4\ell_P^2$ [44]. That is to say, for either neutral or charged particles, the limit of the minimum area change is not zero but a finite value considering the uncertainty principle. The difference between them is to consider the vacuum polarization effect of a black hole for charged particles. Notably, the minimum area changes in both cases are of the same order of magnitude. Thus, due to the quantum effect, the black hole has a uniform discrete area spectrum

$$A = \alpha N \ell_P^2. \quad (1)$$

The phenomenological constant $\alpha \in \mathbf{R}$ is a real number depending on concrete physical conditions, and A is the surface area of the black hole.

For the parameters in Kerr black holes, the mass M , the area A and the angular momentum J , meet the following relation

$$M = \sqrt{\frac{A}{16\pi} + \frac{4\pi J^2}{A}}. \quad (2)$$

In [41], Bekenstein assumes that angular momentum can also be quantized

$$J = \hbar j, \quad (0 \leq j \leq \frac{\alpha N}{8\pi}), \quad (3)$$

where j is a semi-integer. Combining it with the above area quantization in Eq. (1), we can get the discrete energy spectrum of the Kerr black hole

$$M_{N,j} = \sqrt{\hbar} \sqrt{\frac{\alpha N}{16\pi} + \frac{4\pi j^2}{\alpha N}}. \quad (4)$$

Thus, compared with classical black hole, the area-quantized black hole has an energy gap that prevents some energy from entering the black hole.

B. Transition spectral lines and line width

As in the case of the gravitational perturbation around area-quantized black holes in [30], when an area-quantized black hole absorbs a scalar perturbation field with the frequency $\omega_{\hat{n}}$ and modes (l, m) on the Kerr background, where l and m are the orbital and azimuthal numbers, $l \geq 0$ and $-l \leq m \leq l$, it should occur to undergo the transition $M_{N,j} \rightarrow M_{N+\Delta N, j+m}$. Thus,

$$\hbar\omega_{\hat{n}} = M_{N+\hat{n}, j+m} - M_{N,j}, \quad (5)$$

where we set $\Delta N = \hat{n}$, and $\omega_{\hat{n}}$ represents the \hat{n} -th absorption spectral line.

Notably, we do not limit the mode of scalar fields to limit the mode of gravitational waves in [30]. So, the scalar fields possessing different azimuthal numbers will also contribute to the transition.

Through the detailed derivation in the appendix A, we can find if the black hole is a macroscopic black hole, corresponding to the large N limit, the absorption spectra

$$\omega_{\hat{n}} = \frac{\alpha\kappa}{8\pi} \hat{n} + m\Omega_H + O(N^{-1}), \quad (6)$$

where κ and Ω_H are the surface gravity and angular velocity of the Kerr black hole

$$\kappa = \frac{1}{2M} \frac{\sqrt{1-a^2}}{1+\sqrt{1-a^2}}, \quad (7)$$

$$\Omega_H = \frac{1}{2M} \frac{a}{1+\sqrt{1-a^2}}. \quad (8)$$

The dimensionless angular velocity parameter

$$a \equiv J/M^2, \quad 0 \leq a < 1. \quad (9)$$

Additionally, the spectral line possesses the width associated with the spontaneous decay of the black hole energy states for Hawking radiation, just as in atomic physics [45]. In Ref. [46], the analytical fitting function for the line width Γ is given,

$$\Gamma = \frac{1.005}{M} e^{-6.42+1.8a^2+1.9a^{12}-0.1a^{14}}. \quad (10)$$

Thus as the spin of black hole accelerates, the width of absorption spectra also increases.

III. SUPERRADIANT INSTABILITY OF SCALAR FIELD

In this section, we derive the analytical result of the modified growth rate of superradiant instability. We use another set of hypergeometry function bases, which are different from [47], and get a similar result. Next, we model the reflectivity of area-quantized black holes for external scalar fields. And then we consider the case of superradiant scalar fields with different superradiant modes $|nlm\rangle$, where n is the overtone number, l and m are the orbital and azimuthal numbers. We will work in the limit $M/\lambda_\mu = \mu M/\hbar \ll 1$, where μ and M are the mass of the scalar field and the mass of the black hole, respectively.

A. Growth rate of superradiant instability

The metric of the Kerr black hole in Boyer-Linquist coordinates $\{t, r, \theta, \phi\}$ is

$$\begin{aligned} ds^2 = g_{\rho\sigma} dx^\rho dx^\sigma = & - \left(1 - \frac{2Mr}{\Sigma}\right) dt^2 + \frac{\Sigma}{\Delta} dr^2 \\ & + \Sigma d\theta^2 - \frac{2Mar \sin^2 \theta}{\Sigma} dt d\phi \\ & + \left(r^2 + a_*^2 + \frac{2Ma_*^2 r}{\Sigma} \sin^2 \theta\right) \sin^2 \theta d\phi^2, \end{aligned} \quad (11)$$

where M is the black hole mass, and

$$\Sigma = r^2 + a_*^2 \cos^2 \theta, \quad (12)$$

$$\Delta = r^2 - 2Mr + a_*^2 \equiv (r - r_+)(r - r_-). \quad (13)$$

The quantities r_+ and r_- are the radial positions of the outer horizon and the inner horizon, respectively. The angular momentum parameter

$$a_* \equiv J/M = aM. \quad (14)$$

Based on the Kerr background, the massive scalar field ψ obeys the Klein-Gordon equation

$$\nabla^\rho \nabla_\rho \psi = \mu^2 \psi, \quad (15)$$

which can also be written as

$$\frac{1}{\sqrt{-g}} \frac{\partial}{\partial x^\rho} \left(\sqrt{-g} g^{\rho\sigma} \frac{\partial \psi}{\partial x^\sigma} \right) = \mu^2 \psi. \quad (16)$$

where g is the determinant of the Kerr metric $g_{\rho\sigma}$ in Eq. (11), and $g^{\rho\sigma}$ is the inverse metric.

Because of the axial symmetry of the Kerr geometry, the field equation can be separable through the ansatz

$$\psi = e^{-i\omega t + im\phi} S(\theta) R(r). \quad (17)$$

We can get two separate equations for the angular function $S(\theta)$,

$$\frac{1}{\sin\theta} \frac{d}{d\theta} \left(\sin\theta \frac{dS}{d\theta} \right) + \left[a_*^2 (\omega^2 - \mu^2) \cos^2\theta - \frac{m^2}{\sin^2\theta} + \lambda \right] S = 0, \quad (18)$$

and radial function $R(r)$,

$$\Delta \frac{d}{dr} \left(\Delta \frac{dR}{dr} \right) + \left[\omega^2 (r^2 + a_*^2)^2 - 4\omega M r m a_* + m^2 a_*^2 - \Delta (\mu^2 r^2 + a_*^2 \omega^2 + \lambda) \right] R = 0. \quad (19)$$

Here λ is the separation constant and can be determined by Eq. (19) as an eigenvalue of it. Meanwhile, the eigenfunctions $S(\theta)$ are the spheroidal harmonics. Notably, λ is not expressible in analytic form in terms of l and n , and it has an approximate expansion form $l(l+1) + O[a^2(\mu^2 - \omega^2)]$. So if $\omega M \ll 1$ and $\mu M \ll 1$ [9], then the spheroidal harmonics $S(\theta)$ became the spherical harmonics $Y_l^m(\theta)$ and the separation constant

$$\lambda \simeq l(l+1). \quad (20)$$

The angular part $S(\theta)$ of the solution Eq. (17) can be approximated as the well-known spherical harmonics in the above limit. So the key to determining the solution is to solve the radial equation Eq. (19). The radial perturbation equation can be solved by the matched asymptotic expansion [48]. Namely, one divides the radial part into the far region and the near region.

In the appendix B, we solve the radial equation Eq. (19) with matched asymptotic expansion method. Considering $\delta\nu \ll 1$, with $k^2 \equiv \mu^2 - \omega^2$ and $\nu \equiv M\mu^2/k = \nu_0 + \delta\nu$, the eigenfrequency ω is solved as

$$\omega = \mu \left[1 - \left(\frac{M\mu}{\nu_0 + \delta\nu} \right)^2 \right]^{1/2} \simeq \omega_0 + \delta\omega, \quad (21)$$

where $\nu_0 = l + n + 1$ and

$$\begin{aligned} \omega_0 &= \mu \left[1 - \left(\frac{\varepsilon}{\nu_0} \right)^2 \right]^{1/2}, \\ \delta\omega &= \frac{\delta\nu}{M} \left(\frac{\varepsilon}{\nu_0} \right)^3 \left[1 - \left(\frac{\varepsilon}{\nu_0} \right)^2 \right]^{-1/2}. \end{aligned} \quad (22)$$

The gravitational coupling constant has been introduced

$$\varepsilon \equiv M\mu. \quad (23)$$

So we can see when the reflectivity of the black hole is not zero, the growing rate of this scalar cloud is

$$\text{Im}[\delta\omega] = \frac{\delta\nu_*}{M} \left(\frac{\varepsilon}{\nu_0}\right)^3 \left[1 - \left(\frac{\varepsilon}{\nu_0}\right)^2\right]^{-1/2} \frac{1 - \mathcal{R}^2}{1 + \mathcal{R}^2 + 2\mathcal{R} \cos(i \sum_{j=1}^l \ln \frac{j+2ip}{j-2ip})}, \quad (24)$$

where

$$\delta\nu_* = \frac{2p}{n!} \left[\frac{l!}{(2l)!(2l+1)!} \right]^2 \prod_{j=1}^l (j^2 + 4p^2) (2l+n+1)! [2k(r_+ - r_-)]^{2l+1}. \quad (25)$$

B. Reflectivity with discrete feature

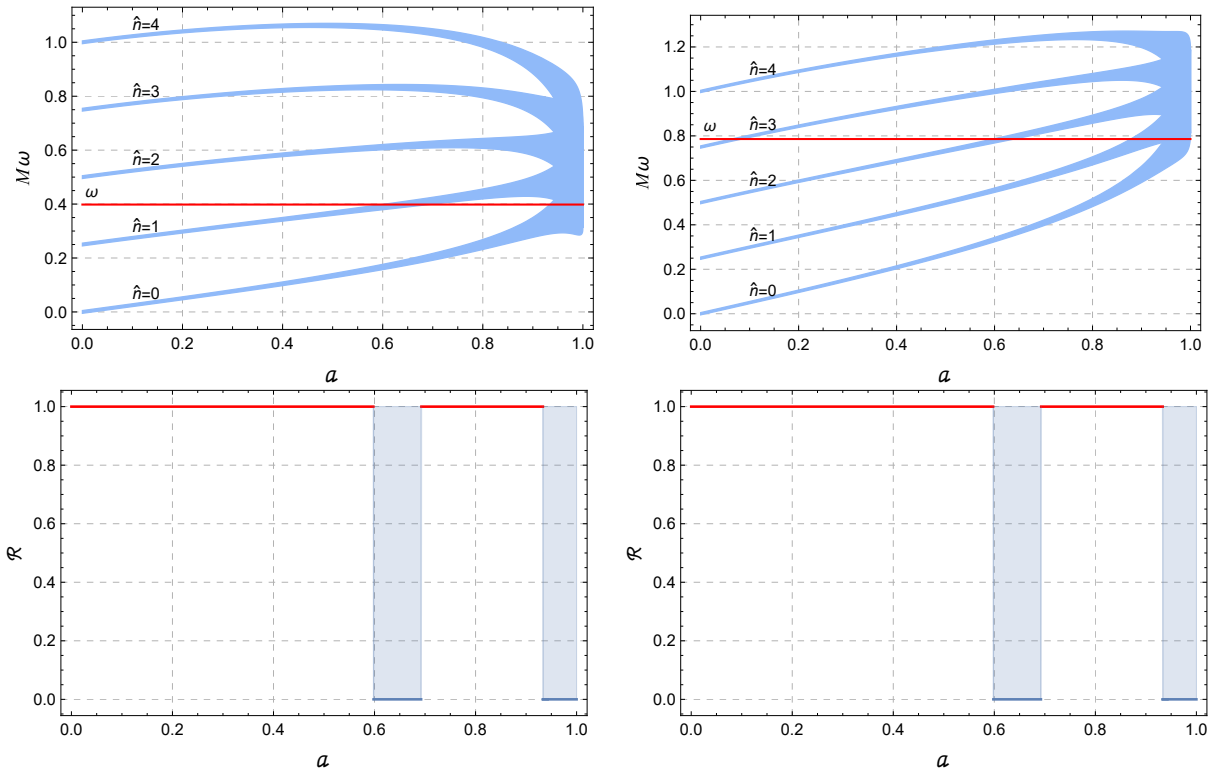


FIG. 1: The left set of pictures is about the absorption of the scalar fields with $m = 1$ by area-quantized black holes. And the right set of pictures is about the absorption of the scalar fields with $m = 2$ by the black holes. In the top pictures, the blue region represents the absorption spectrum of the area-quantized black holes, and the red line represents the angular frequency of the scalar fields. In the bottom pictures, the blue and red lines correspond to the parts where the red line passes through and does not pass through the blue region in the top pictures, respectively

The scalar fields can be absorbed by low-spin area-quantized black holes only at characterized frequencies $f_{\hat{n}} = \omega_{\hat{n}}/2\pi$, while at other frequencies fully be reflected. As the spin of the area-quantized black holes continues to increase, the Hawking effect also continues to strengthen. So

we need to consider the width of the absorption lines, and then the scalar fields can be absorbed by high-spin area-quantized black holes in the frequency range $f_{\hat{n}} - \Gamma/2 < f < f_{\hat{n}} + \Gamma/2$.

The reflectivity is zero in the frequency range $f_{\hat{n}} - \Gamma/2 < f < f_{\hat{n}} + \Gamma/2$, and the reflectivity is one beyond the frequency range. Thus, the reflectivity \mathcal{R} can be modeled as follow:

$$\mathcal{R} = \begin{cases} 1 - |\Theta(\sin \zeta_1) - \Theta(\sin \zeta_2)|, & \Delta\omega > 2\pi\Gamma \\ 0, & \Delta\omega \leq 2\pi\Gamma \end{cases} \quad (26)$$

where

$$\zeta_1 = \frac{\pi(\omega - m\Omega_H + 2\pi\Gamma/2)}{\Delta\omega}, \quad (27)$$

$$\zeta_2 = \frac{\pi(\omega - m\Omega_H - 2\pi\Gamma/2)}{\Delta\omega}, \quad (28)$$

and $\Theta(\varphi)$ is the unit step function and $\Delta\omega = \alpha\kappa/8\pi$ is the gap of absorption spectra.

Notably, the reflectivity set in Ref. [46] differs from what we set in this work. In Ref. [46], the reflectivity set by them is characterized by pulses, not within the characterized frequency range. They suggest that the reflectivity is not one when gravitational fields absolutely cannot be absorbed by area-quantized black holes. However, the reflectivity should be a constant 1 rather than some pulses beyond the characterized frequencies range.

In Fig. 1, we plot the frequency ω of scalar fields and the absorption spectral lines with $m = 1$ and 2 as a function of the spin parameter a of area-quantized black holes in the top picture and the corresponding reflectivity \mathcal{R} in the bottom picture. Notice that the black holes have different absorption spectra for the scalar fields with different azimuthal numbers m . In addition, as the rotation of the black holes accelerates, the linewidth will continue to increase. When the linewidth increases to larger than the absorption frequency gap $\Delta\omega = \alpha\kappa/8\pi$, all the spectral lines overlap. Through our calculation, we found only the critical dimensionless spin parameter $a_{\text{crit}} \geq 0.9430$, the absorption spectra overlap. Area-quantized black holes can recover into classical black holes. It is worth noting that the overlap is not related to the mass of the black holes and external fields from Eq. (6) and Eq. (10).

Furthermore, if the scalar fields can be superradiated, we generally call them superradiant scalar fields. Their frequencies of superradiant modes $|nlm\rangle$ can be characterized by ω_0 in Eq. (22)

$$f_{nlm} \equiv \frac{\omega_0}{2\pi} = \frac{\varepsilon}{2\pi M} \left(1 - \frac{\varepsilon^2}{l+n+1} \right). \quad (29)$$

Then they should meet the superradiance condition

$$\omega - m\Omega_H < 0. \quad (30)$$

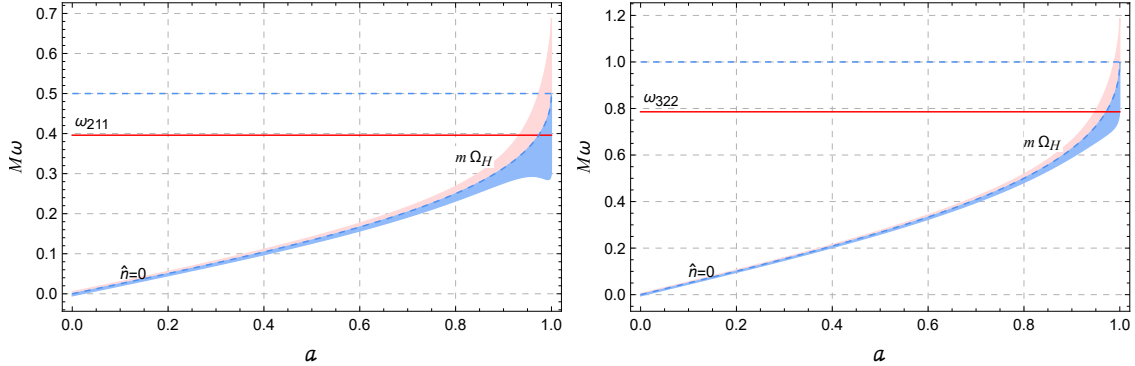


FIG. 2: The set of pictures is about the absorption of the superradiant scalar fields. The left picture is for the scalar fields with the superradiant mode $|211\rangle$, and the right image is for the scalar field with the superradiant mode $|322\rangle$. The blue dashed curve represents the first absorption spectral line and the limit of superradiance. The red region is the upper broadening part of the first absorption spectral line. In this region, the area-quantized black holes fully reflect the superradiant scalar fields. The blue region is the lower broadening part. It represents that the area-quantized black holes can fully absorb the superradiant scalar fields in this region. Lastly, the red line is the angular frequency of the superradiant scalar fields. The blue dashed line represents the first absorption spectral line and the upper limit angular frequency of all superradiant scalar fields with the specific m .

However, from Eq. (6) the first absorption spectral line of area-quantized black holes is

$$\omega_{\hat{n}=0} = m\Omega_H. \quad (31)$$

So only when the frequencies of superradiant scalar fields f_{nlm} are in the frequency range $f_{\hat{n}} - \Gamma/2 < f < f_{\hat{n}} + \Gamma/2$ and $f_{nlm} < f_{\hat{n}=0} = \omega_{\hat{n}=0}/2\pi$, the area-quantized black holes can absorb the superradiant scalar fields to transition to the higher energy level. In other words, the red line that represents the frequency of superradiant scalar fields only passes through the first absorption spectral line one time. From the physical perspective, only the area-quantized black holes in a small region of the spin can absorb the superradiant scalar fields.

IV. SCALAR CLOUD AROUND AREA-QUANTIZED BLACK HOLE

In this section, we consider the effect of scalar clouds from the area quantization of black holes. The area quantization of black holes can cause the scalar fields to have superradiant instability around area-quantized black holes only if the spin of these black holes is slightly greater than the superradiance condition. The formation of the scalar clouds is suppressed around area-quantized black holes with a spin outside the above range. As a result, the initial maximum spin of area-

quantized black holes with scalar clouds is smaller than in the case of classical black holes. Then the scalar clouds formed near the area-quantized black holes are lighter than those near the corresponding classical black holes. Additionally, the area-quantized black holes with a specific spin only absorb the scalar fields that meet the energy gap of the black holes. Thus, the limited mass range of the scalar fields leads to the Bohr radius of the limited scalar clouds.

A. Suppression and mass of scalar cloud

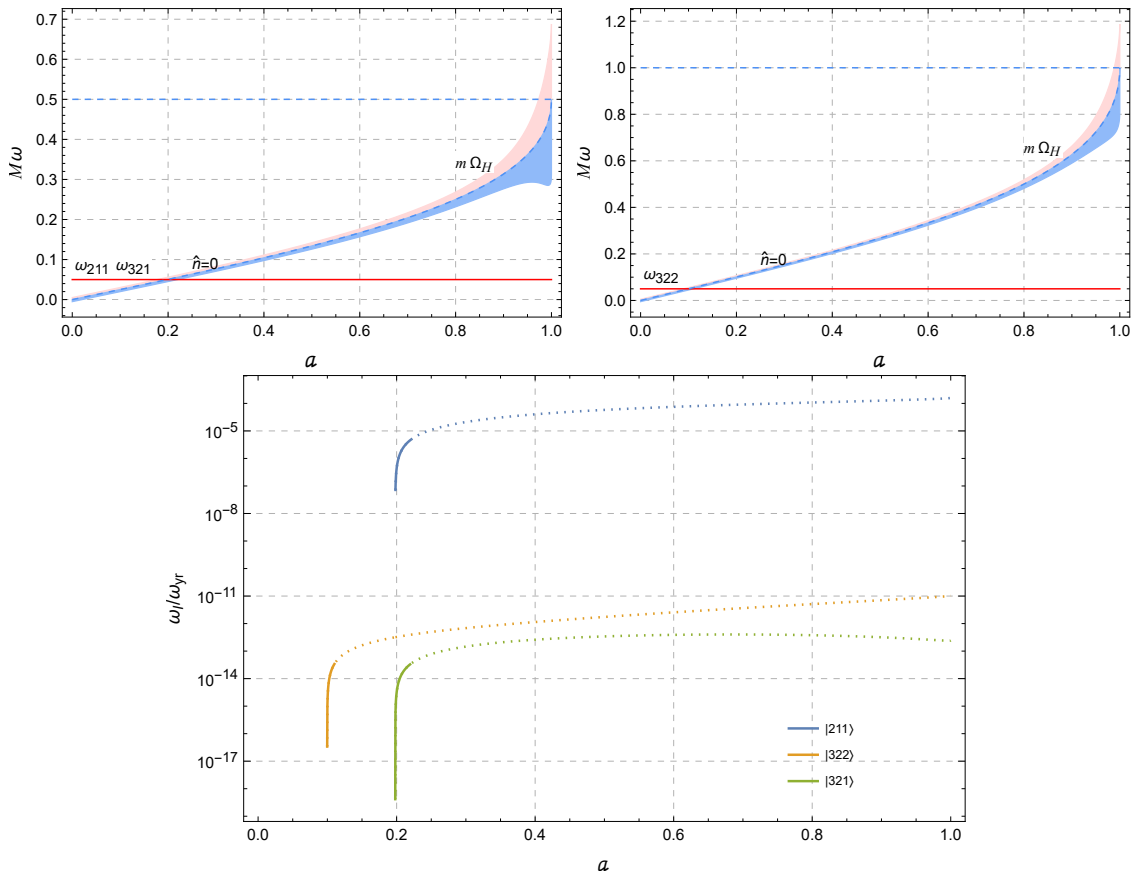


FIG. 3: We have plotted the growth rates $\omega_I/\omega_{\text{yr}}$ of the fundamental modes $|211\rangle$, $|322\rangle$ and $|321\rangle$ as a function of the spin parameter a of area-quantized black holes with $M = 60M_\odot$ in the bottom picture. The dotted curves represent the growth rate for classical black holes and the solid curves represent that for area-quantized ones. In addition, the top two pictures represent the absorption situation of the area-quantized black holes for the superradiant scalar fields. It is clearly seen that the cross part of the top two pictures matches well with the solid curves of the bottom picture.

In Fig. 3, we plot the superradiance growth rates $\omega_I \equiv \text{Im}[\delta\omega]$ in Eq. (22) of different three fundamental modes $|nlm\rangle$ as a function of the spin parameter a . It is normalised by $\omega_{\text{yr}} \equiv 2\pi/T_{\text{yr}}$,

and T_{yr} is the time for one year. By matching the top two pictures and the bottom picture in Fig. 3, we can find that the part where the red line passes through the blue region in the top pictures corresponds to the remaining growth rate of scalar clouds for area quantization in the bottom picture. From a physical point of view, the area-quantized black holes are like classical black holes for the superradiant scalar fields in this crossing region. Thus, the scalar fields have superradiant instability around these area-quantized black holes and form the scalar cloud. However, some area-quantized black holes can not absorb the superradiant scalar fields. These area-quantized black holes are mirrors for these superradiant scalar fields. Thus, the scalar fields do not have the superradiant instability around these black holes. And the growth rate of the scalar cloud is zero. Namely, there are no scalar clouds around these area-quantized black holes.

For example, we can see that for the black holes with a slightly larger spin, such as $a = 0.4$, a scalar cloud should form in the case of classical black holes, while no scalar cloud forms at this time from the bottom picture. That is to say, the formation of the scalar clouds around some area-quantized black holes is suppressed. It is worth noting that the superradiant modes with the same magnetic quantum number m , such as the $|211\rangle$ and $|321\rangle$ modes, can have the same angular frequency from the top pictures. They have different growth rates of superradiant instability depending on other quantum numbers from the bottom picture.

In addition, the scalar clouds that form around area-quantized black holes should be lighter. Because these scalar fields only have superradiant instability around the area-quantized black holes near the lower limit of superradiance condition, $\omega_{nlm} = m\Omega_H$. For example, except for the $|211\rangle$ mode, the growth period of the $|322\rangle$ and $|321\rangle$ modes is much larger than the cosmic age in the bottom picture, So we only consider the $|211\rangle$ mode. For the $|211\rangle$ mode, the scalar clouds only can form around the black hole with $a = 0.220$. As the scalar cloud spins down the black hole, the growth rate of the mode becomes zero until the spin of the black hole drops to $a = 0.198$, namely $\omega_{211} = m\Omega_H$.

Here, we can estimate the mass of the scalar cloud with $|211\rangle$ mode around the area-quantized black hole with $60M_\odot$. Because the rate of gravitational wave radiation from the scalar cloud is slower than the growth rate of the scalar cloud, we can ignore the gravitational wave radiation. At this point, the mass and angular momentum of the black hole and the scalar cloud are conserved, namely

$$M_{\text{cloud}} = M_i - M_f, \quad J_{\text{cloud}} = J_i - J_f, \quad (32)$$

where M_{cloud} and J_{cloud} are the mass and angular momentum of the scalar cloud, and M_i and M_f

are the initial and final mass of the black hole.

At infinity, the scalar field is composed of many quanta each with the energy $E = \hbar\omega_{211}$ and the angular momentum $J = \hbar m$. Therefore, the ratio of the angular momentum and the energy carried by the scalar field is m/ω , namely

$$\frac{\Delta J}{\Delta M} = \frac{m}{\omega_{211}}. \quad (33)$$

Substitute it into Eq. (32), we can get

$$\frac{m}{\omega_{211}}(M_i - M_f) = J_i - J_f. \quad (34)$$

And the scalar cloud stops growing. The superradiant instability is saturated

$$\omega_{211} = m\Omega_H. \quad (35)$$

We substitute Eq. (35) and Eq. (8) into Eq. (34), and get the final mass of the black hole

$$M_f = \frac{m^3 - \sqrt{m^6 - 16m^2\omega_{211}^2 M_i^2 (m - \omega_{211} M_i a_i)^2}}{8\omega_{211}^2 M_i (m - \omega_{211} M_i a_i)}, \quad (36)$$

where a_i is the initial spin parameter of the black hole. Because of $\varepsilon \ll 1$ in ω_{211} , the first order approximate expression of the final mass is

$$M_f \approx M_i - \frac{M_i^2 a_i \omega_{211}}{m} + O(\varepsilon). \quad (37)$$

So the mass of the scalar cloud is

$$M_{cloud} = \frac{M_i^2 a_i \omega_{211}}{m} = \frac{a_i \varepsilon}{m} \left(1 - \frac{\varepsilon^2}{l+n+1} \right) M_i, \quad (38)$$

namely

$$\frac{M_{cloud}}{M_i} = 1.1\%. \quad (39)$$

Thus, the mass of the scalar cloud with the $|211\rangle$ mode around the area-quantized black holes with $60M_\odot$ is $0.66M_\odot$. From the dashed curve part of the bottom picture, we can see if the black hole is a classical black hole, its initial spin parameter a_i can be 0.8. Then the mass of the scalar cloud is $2.4M_\odot$, which is 3.6 times that of an area-quantized black hole scenario. We can see the smaller frequency of the superradiant scalar fields, the smaller maximum initial spin parameter of the area-quantized black holes that can superradiant them, and the smaller mass of the scalar clouds.

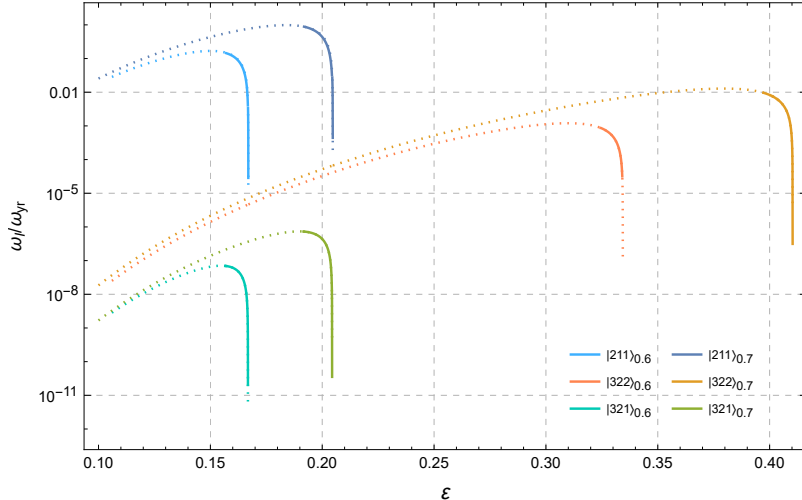


FIG. 4: We plot the superradiance growth rates ω_I/ω_{yT} in Eq. (22) of different three fundamental modes as a function of the gravitational coupling constant ε for two black hole spin parameters $a = 0.6$ and $a = 0.7$. The dotted curves represent the growth rates of the scalar clouds for classical black holes and the solid curves represent the case for area-quantized black holes.

B. Bohr radius of scalar cloud

Through the calculation in Sec. III A, we can approximate the scalar cloud and black hole system as a “gravitational atom” for $\varepsilon \ll 1$. Therefore, the scalar cloud has a Bohr radius,

$$r_c \equiv \frac{\lambda_\mu}{\varepsilon} = \frac{M}{\varepsilon^2}, \quad (40)$$

which characterizes the characteristic distance of the scalar cloud relative to the black hole in space. If we set the scale of the black hole, different ε depend on the different characteristic distances of a scalar cloud.

In Fig. 4, we can see whether the spin parameter of the black hole is 0.6 or 0.7, the $|211\rangle$ and $|321\rangle$ modes have the same range of ε . It is because the absorption spectrum of the area-quantized black hole is the same for the scalar clouds with the same azimuth number m . That is to say, the scalar clouds with the $|211\rangle$ and $|321\rangle$ modes have the same Bohr radius. Their center is equally far from the black hole. For example, in the case of $a = 0.7$, we set $\varepsilon = 0.2$. Then the Bohr radius of the $|211\rangle$ and $|321\rangle$ modes is

$$r_c = \frac{M}{0.2^2} = 25M. \quad (41)$$

For the $|322\rangle$ mode, its azimuth number $m = 2$ is greater than the other two modes. The absorption spectral lines of an area-quantized black hole as a function of the spin parameter a are steeper. So,

the scalar fields have superradiant instability at a higher frequency around the black holes with specific spin. From Fig. 4, we can see ε is probably around 0.4 for the $|322\rangle$ mode in case of $a = 0.7$. At this point, the Bohr radius of the scalar clouds is

$$r_c = \frac{M}{0.4^2} = 6.25M. \quad (42)$$

So the scalar clouds with $m = 2$ are generally about 4 times closer to the area-quantized black hole than the scalar clouds with $m = 1$.

In addition, by comparing the cases of $a = 0.6$ and $a = 0.7$ in Fig. 4, we can see that the scalar clouds around the area-quantized black holes with the higher spin have a smaller Bohr radius. In other words, a higher spin area-quantized black hole will result in a closer scalar cloud around it. For example, we consider about the $|211\rangle$ and $|321\rangle$ modes. In case of $a = 0.6$, we set $\varepsilon = 0.16$, and the Bohr radius is

$$r_c = \frac{M}{0.16^2} = 39M. \quad (43)$$

Therefore, the Bohr radius of the scalar clouds in case of $a = 0.7$ is $14M$ smaller than that in case of $a = 0.6$ for $|211\rangle$ and $|321\rangle$.

V. CONCLUSION

Based on Bekenstein and Mukhanov's proposal [31], an area-quantized black hole possesses non-zero and discrete reflectivity for external scalar field. The non-zero reflectivity will affect the absorption of scalar fields by area-quantized black holes. If these scalar fields can also be superradiated by the black holes, the area quantization of the black hole can limit the superradiant instability of the scalar fields around area-quantized black holes. In this work, we derive the corrective growth rate of scalar clouds by solving the massive scalar field perturbation equation on the Kerr background analytically. And we model the reflectivity of area-quantized Kerr black holes for massive scalar fields. We show that scalar fields can be absorbed by area-quantized black holes only within the absorption spectrum of the area-quantized black holes. This corresponds to the reflectivity of $R = 0$, indicating the complete absorption. In all other cases, the fields are fully reflected, with the reflectivity of $R = 1$. Due to superradiance conditions, superradiant scalar fields can only be within the first absorption spectral line of area-quantized black holes. In other words, area-quantized black holes only in a small range of the spin absorb superradiant scalar fields. Finally, we study the effect of scalar clouds around area-quantized black holes for the above reasons.

We found that the area quantization of black holes can result in the suppression of scalar clouds for area-quantized black holes. And because the mass and angular momentum of the scalar field and the black hole are conserved, we can estimate the mass of the scalar clouds around area-quantized black holes. We found that the smaller the frequency of the scalar fields, the smaller the maximum initial spin parameter of the area-quantized black holes which can superradiate them, and the smaller the mass of the scalar clouds. In the example we provided above, the mass of the scalar clouds around area-quantized black holes is only 0.28 times that of the classical black hole scenario. In addition, scalar clouds have a narrow range of the distance from the area-quantized black hole with a specific spin. It is because the discrete mass level gap of area-quantized black holes selects the scalar fields with matching energy. We found that the scalar cloud with larger m is closer to the area-quantized black hole and a higher spin black hole tends to result in a closer scalar cloud around it. The scalar clouds surrounding the black holes can radiate gravitational waves or even the fast radio bursts [49, 50], which provides interesting gravitational phenomenology of astronomical observations [51, 52]. It will also be interesting to consider the vector or tensor condensates [53, 54]. In the following work, we hope to study these effects of area quantization to effectively probe those astrophysical black hole systems.

Acknowledgments

This work is supported by the National Key Research and Development Program of China (No. 2023YFC2206200), the National Natural Science Foundation of China under Grant No.12375059.

Appendix A: The absorption approximate formula

Here we derive the absorption approximate formula in Eq. (5) under a large N limit. Approximately, Eq. (4) can be expanded as

$$\begin{aligned} M_{N+\Delta N, j+\Delta j} &= \sqrt{\hbar} \sqrt{\frac{\alpha(N+\Delta N)}{16\pi} + \frac{4\pi(j+\Delta j)^2}{\alpha(N+\Delta N)}} \\ &\simeq M_{N,j} + \frac{\partial M_{N,j}}{\partial N} \Delta N + \frac{\partial M_{N,j}}{\partial j} \Delta j + O\left(\frac{\Delta N}{N}, \frac{\Delta j}{j}\right). \end{aligned} \quad (\text{A1})$$

Substituting the above equation into Eq. (5), we get

$$\begin{aligned} M_{N+\Delta N, j+\Delta j} - M_{N,j} &\simeq \frac{\partial M_{N,j}}{\partial N} \Delta N + \frac{\partial M_{N,j}}{\partial j} \Delta j \\ &= \frac{1}{2M} \left(\frac{\hbar\alpha}{16\pi} - \frac{4\pi\hbar j^2}{\alpha N^2} \right) \Delta N + \frac{1}{2M} \left(\frac{8\pi\hbar j}{\alpha N} \right) \Delta j. \end{aligned} \quad (\text{A2})$$

Consider the following relations

$$A = 8\pi M^2(1 + \sqrt{1 - a^2}), \quad (\text{A3})$$

$$j = \frac{aM^2}{\hbar}, \quad (0 \leq j \leq \frac{\alpha N}{8\pi}), \quad (\text{A4})$$

$$N = A/\hbar\alpha, \quad (\text{A5})$$

the first term in Eq. (A2) becomes

$$\frac{1}{2M} \left(\frac{\hbar\alpha}{16\pi} - \frac{4\pi\hbar j^2}{\alpha N^2} \right) = \frac{\hbar\alpha}{16\pi M} \frac{\sqrt{1 - a^2}}{1 + \sqrt{1 - a^2}} = \frac{\hbar\alpha\kappa}{8\pi}, \quad (\text{A6})$$

where $\kappa \equiv \frac{1}{2M} \frac{\sqrt{1 - a^2}}{1 + \sqrt{1 - a^2}}$ is the surface gravitation of the Kerr black hole. The second term in Eq. (A2) becomes

$$\frac{1}{2M} \left(\frac{8\pi\hbar j}{\alpha N} \right) = \frac{\hbar a}{2M(1 + \sqrt{1 - a^2})} = \hbar\Omega_H, \quad (\text{A7})$$

where $\Omega_H \equiv \frac{1}{2M} \frac{a}{1 + \sqrt{1 - a^2}}$ is the surface angular velocity of the Kerr black hole.

So with $\Delta N = \hat{n}$, $\Delta j = m$, we can get

$$\begin{aligned} \hbar\omega_{\hat{n}} &\simeq \frac{\partial M_{N,j}}{\partial N} \Delta N + \frac{\partial M_{N,j}}{\partial j} \Delta j + O\left(\frac{\Delta N}{N}, \frac{\Delta j}{j}\right) \\ &\simeq \hbar\hat{n} \frac{\alpha\kappa}{8\pi} + \hbar m\Omega_H + O(N^{-1}). \end{aligned} \quad (\text{A8})$$

Furthermore, due to the correspondence principle, the approximate expansion also indeed satisfies the macroscopic first law of Kerr black hole

$$dM = \frac{\kappa}{8\pi} dA + \Omega_H dJ = \hbar\hat{n} \frac{\kappa\alpha}{8\pi} + \hbar m\Omega_H, \quad (\text{A9})$$

which is consistent with (A8) considering $dM = \hbar\omega_{\hat{n}}$.

Appendix B: Solving the radial equation

In this appendix, we solve the radial equation (19) with the matched asymptotic expansion method, which includes the far region, the near region, and the overlap region solutions.

1. The far region solution

In the far region, where the influence from the black hole can be ignored, the equation can be approximated to a Schrödinger-like equation with a Newtonian potential. In the far region limit, $r \gg M$ and $r \sim l/\omega$, the terms in the radial equation Eq. (19) can be approximated as

$$\frac{\Delta\omega^2 a_*^2}{r^4} \sim 0, \quad \frac{\omega M m a_*}{r^3} \sim 0, \quad \frac{m^2 a_*^2}{r^4} \sim 0, \quad (\text{B1})$$

$$\frac{\omega^2(a_*^2 + r^2)^2}{r^4} \simeq \omega^2, \quad \frac{\Delta\mu^2 r^2}{r^4} \simeq \mu^2 \left(1 - \frac{2M}{r}\right), \quad (\text{B2})$$

$$\frac{\Delta \frac{d}{dr} \left(\Delta \frac{dR}{dr}\right)}{r^4} \simeq \frac{d^2 R}{dr^2} + \frac{2}{r} \frac{dR}{dr}, \quad \frac{\Delta l(l+1)}{r^4} \simeq \frac{l(l+1)}{r^2}. \quad (\text{B3})$$

Then the radial equation Eq. (19) can be approximated to the radial hydrogen atom like equation

$$\frac{d^2(rR)}{dr^2} + \left[\omega^2 - \mu^2 \left(1 - \frac{2M}{r}\right) - \frac{l(l+1)}{r^2} \right] (rR) = 0. \quad (\text{B4})$$

After setting $\rho = 2kr$, we obtain

$$\frac{d^2(\rho R)}{d\rho^2} + \left[-\frac{1}{4} + \frac{\nu}{\rho} - \frac{l(l+1)}{\rho^2} \right] (\rho R) = 0, \quad (\text{B5})$$

where the notations

$$k \equiv \sqrt{\mu^2 - \omega^2}, \quad \nu \equiv M\mu^2/k. \quad (\text{B6})$$

The solution of Eq. (B5) is $\rho R(\rho) = e^{-\rho/2} \rho^{l+1} F(l+1-\nu, 2l+2; \rho)$, namely

$$R(r) = (2kr)^l e^{-kr} F(l+1-\nu, 2l+2; 2kr), \quad (\text{B7})$$

where $F(l+1-\nu, 2l+2; 2kr)$ is the confluent hypergeometric function.

Unlike the boundary condition of the electron wave function in the hydrogen atom, which is located at the origin, the inner boundary condition of this problem is located at the event horizon, which corresponds to absorption by the black hole. So the eigenvalues ω should be the complex formula and have corresponding complex ν [55], which satisfy

$$\nu = \nu_0 + \delta\nu, \quad \nu_0 \equiv n + l + 1, \quad (\text{B8})$$

where $\delta\nu$ is a small complex correction. Then, the solution in Eq. (B7) also can be expressed as

$$R(r) = (2kr)^l e^{-kr} F(-n - \delta\nu, 2l+2; 2kr). \quad (\text{B9})$$

2. The near region solution

In the near region, namely the region close to the event horizon, the solution contains the information about the event horizon of the black hole. Because $r = r_+$ is the singularity of the radial equation, as r close to the event horizon, the function R in radial equation Eq. (19) varies very rapidly. It is convenient to introduce the rescaled radial coordinate to accommodate this rapid change

$$z \equiv \frac{r - r_+}{r_+ - r_-}, \quad \Delta = z(z+1)(r_+ - r_-)^2. \quad (\text{B10})$$

When $r \ll l/\omega$ or $r \ll l/\mu$, namely $z \ll l/\omega(r_+ - r_-)$ or $z \ll l/\mu(r_+ - r_-)$, then

$$\begin{aligned}\Delta\mu^2r^2 &= z(z+1)\mu^2r^2/(r_+ - r_-) \ll \Delta l(l+1), \\ \Delta a_*^2\omega^2 &= z(z+1)\omega^2a_*^2/(r_+ - r_-) \ll \Delta l(l+1).\end{aligned}\tag{B11}$$

So in Eq. (19), the term

$$\Delta(\mu^2r^2 + a_*^2\omega^2 + \lambda) \simeq \Delta\lambda \simeq \Delta l(l+1).\tag{B12}$$

Meanwhile, in the near region,

$$4\omega Mrma_* \simeq 4\omega Mr_+ma_*,\tag{B13}$$

and

$$\omega^2(r^2 + a_*^2)^2 \simeq \omega^2(r_+^2 + a_*^2)^2 = (2\omega Mr_+)^2,\tag{B14}$$

we get

$$\omega^2(r^2 + a_*^2)^2 - 4\omega Mrma_* + m^2a_*^2 \simeq (ma_* - 2\omega Mr_+)^2.\tag{B15}$$

Then the radial equation in Eq. (19) can be approximated as

$$z(z+1)\frac{d}{dz}\left[z(z+1)\frac{dR}{dz}\right] + [p^2 - l(l+1)z(z+1)]R = 0,\tag{B16}$$

where the dimensionless quantity

$$p \equiv \frac{ma_* - 2\omega Mr_+}{r_+ - r_-}.\tag{B17}$$

In this differential equation (B16), there are three regular singularities $\{0, -1, \infty\}$. We can determine the Riemann P form of the solutions of Eq. (B16) by their index equations

$$x_n(x_n - 1) + A_n + B_n = 0,\tag{B18}$$

where x_n is the index of linear independent series solutions. A_n is the first order characteristic coefficient and B_n is the second order characteristic coefficient for n -th singularity. Substituting

$$\begin{aligned}A_0 &= 1, & B_0 &= p^2, \\ A_{-1} &= 1, & B_{-1} &= p^2, \\ A_\infty &= 0, & B_\infty &= -l(l+1),\end{aligned}\tag{B19}$$

we can get the indexes

$$\begin{aligned} x_0^\pm &= \pm ip, & x_{-1}^\pm &= \pm ip, \\ x_\infty^+ &= l+1, & x_\infty^- &= -l. \end{aligned} \tag{B20}$$

So the solution of Eq. (B16) is

$$R(z) = P \left\{ \begin{array}{ccc} 0 & -1 & \infty \\ ip & -ip & -l \\ -ip & ip & l+1 \end{array} ; z \right\} \tag{B21}$$

$$= \left(\frac{z}{z+1} \right)^{ip} P \left\{ \begin{array}{ccc} 1 & 0 & \infty \\ 0 & 0 & -l \\ -2ip & 2ip & l+1 \end{array} ; z+1 \right\} \tag{B22}$$

$$= \left(\frac{z}{z+1} \right)^{ip} F(-l, l+1, 1-2ip; z+1), \tag{B23}$$

where Eq. (B22) is the *Riemann P equation* [56].

The hypergeometry function $F(-l, l+1, 1-2ip; z+1)$ can be expressed by two linear independent solutions,

$$\begin{aligned} &F(-l, l+1, 1-2ip; z+1) \\ &= P \left\{ \begin{array}{ccc} 1 & 0 & \infty \\ 0 & 0 & -l \\ -2ip & 2ip & l+1 \end{array} ; z+1 \right\} \\ &= (-z^{-1})^{-l} P \left\{ \begin{array}{ccc} \infty & 1 & 0 \\ -l & 0 & 0 \\ -l-2ip & 2ip & 2l+1 \end{array} ; -z^{-1} \right\} \\ &= (-z)^l F(-l, -l-2ip, -2l, -z^{-1}) \equiv U_3, \end{aligned} \tag{B24}$$

and

$$\begin{aligned}
& F(-l, l+1, 1-2ip; z+1) \\
&= P \left\{ \begin{array}{ccc} 1 & 0 & \infty \\ 0 & 0 & -l \\ -2ip & 2ip & l+1 \end{array} ; z+1 \right\} \\
&= (-z^{-1})^{l+1} P \left\{ \begin{array}{ccc} \infty & 1 & 0 \\ l+1 & 0 & -2l-1 \\ l+1-2ip & 2ip & 0 \end{array} ; -z^{-1} \right\} \\
&= (-z)^{-l-1} F(l+1, l+1-2ip, 2l+2, -z^{-1}) \equiv U_4.
\end{aligned} \tag{B25}$$

So the solution of Eq. (B16) can be expressed as follows,

$$R(z) = \left(\frac{z}{z+1} \right)^{ip} F(-l, l+1, 1-2ip; z+1) \tag{B26}$$

$$= A \left(\frac{z}{z+1} \right)^{ip} U_3 + B \left(\frac{z}{z+1} \right)^{ip} U_4, \tag{B27}$$

where A and B are the expansion coefficient of U_3 and U_4 respectively.

U_3 and U_4 cannot be represented as the ingoing and outgoing solutions, but two other linear combinations of them U_1 and U_5 can,

$$(U_3, U_4) = (U_1, U_5) \begin{pmatrix} f_{13} & f_{14} \\ f_{53} & f_{54} \end{pmatrix}, \tag{B28}$$

where

$$U_1 = {}_2F_1(-l, l+1, 1+2ip; -z), \tag{B29}$$

$$U_5 = (-z)^{-2ip} {}_2F_1(-l-2ip, l+1-2ip, 1-2ip; -z), \tag{B30}$$

and

$$f_{13} = (-1)^l \frac{\Gamma(-2l)\Gamma(-2ip)}{\Gamma(-l)\Gamma(-2ip-l)}, \tag{B31}$$

$$f_{53} = (-1)^l \frac{\Gamma(-2l)\Gamma(2ip)}{\Gamma(-l+2ip)\Gamma(-l)}, \tag{B32}$$

$$f_{14} = (-1)^{1-l} \frac{\Gamma(2l+2)\Gamma(-2ip)}{\Gamma(l+1)\Gamma(l-2ip+1)}, \tag{B33}$$

$$f_{54} = (-1)^{1-l} \frac{\Gamma(2l+2)\Gamma(2ip)}{\Gamma(l+1)\Gamma(l+2ip+1)}. \tag{B34}$$

Finally, the radial solution of Eq. (B16) can be expressed as

$$R(z) = A \left(\frac{z}{z+1} \right)^{ip} U_3 + B \left(\frac{z}{z+1} \right)^{ip} U_4 \tag{B35}$$

$$= \left(\frac{z}{z+1} \right)^{ip} (U_1, U_5) \begin{pmatrix} f_{13} & f_{14} \\ f_{53} & f_{54} \end{pmatrix} \begin{pmatrix} A \\ B \end{pmatrix}. \quad (\text{B36})$$

Using the boundary condition of the event horizon, the reflectivity is

$$\mathcal{R} = \frac{Af_{53} + Bf_{54}}{Af_{13} + Bf_{14}}. \quad (\text{B37})$$

We can get the relation between A and B through the above equation

$$A = B \left(\frac{f_{54} - \mathcal{R}f_{14}}{\mathcal{R}f_{13} - f_{53}} \right). \quad (\text{B38})$$

3. The overlap region solution

In the overlap region, we connect the solutions in the near region with the ones in the far region to derive the physical solutions. For the property of confluent hypergeometric functions

$$\begin{aligned} & F(-n - \delta\nu, 2l + 2; 2kr) \\ &= \frac{\Gamma(-2l - 1)}{\Gamma(-n - \delta\nu - 2n - 1)} F(-n - \delta\nu, 2l + 2; 2kr) \\ &+ \frac{(2kr)^{-2l-1} \Gamma(2l + 1)}{\Gamma(-n - \delta\nu)} F(-n - \delta\nu - 2l - 1, -2l; 2kr), \end{aligned} \quad (\text{B39})$$

and Gamma functions

$$\frac{\Gamma(-2l - 1)}{\Gamma(-n - \delta\nu - 2l - 1)} = (-1)^n \frac{\Gamma(2l + n + 2)}{\Gamma(2l + 2)}, \quad (\text{B40})$$

$$\frac{\Gamma(2l + 1)}{\Gamma(-n - \delta\nu)} = (-1)^{n+1} \delta\nu \Gamma(n + 1) \Gamma(2l + 1). \quad (\text{B41})$$

So the near asymptotic expansion behavior of the far solutions in the overlap region at $2kr \rightarrow 0$ is

$$\begin{aligned} R(r) &= (2kr)^l e^{-kr} F(-n - \delta\nu, 2l + 2; 2kr) \\ &\simeq (-1)^n \frac{\Gamma(2l + n + 2)}{\Gamma(2l + 2)} (2kr)^l + \\ &(-1)^{n+1} \Gamma(n + 1) \Gamma(2l + 1) \delta\nu (2kr)^{-l-1}. \end{aligned} \quad (\text{B42})$$

Meanwhile, when $r \gg M$ for

$$U_3 \simeq (-z)^l = \left(\frac{-r}{r_+ - r_-} \right)^l, \quad (\text{B43})$$

$$U_4 \simeq (-z)^{-l-1} = \left(\frac{-r}{r_+ - r_-} \right)^{-l-1}, \quad (\text{B44})$$

the remote asymptotic behavior the near solutions in the overlap region is

$$R(r) \simeq A \left(\frac{-r}{r_+ - r_-} \right)^l + B \left(\frac{-r}{r_+ - r_-} \right)^{-l-1}. \quad (\text{B45})$$

These two solutions, Eq. (B42) and Eq. (B45), can be matched to determine A and B in the overlap region. Considering the relation between A and B in Eq. (B38), we can derive the formula of $\delta\nu$

$$\begin{aligned}
\delta\nu &= \frac{[2k(r_+ - r_-)]^{2l+1}\Gamma(-2l)\Gamma(l+1)(\Gamma(2l+n+2))}{\Gamma(-l)\Gamma(2l+1)\Gamma(2l+2)^2\Gamma(n+1)} \\
&\times \frac{\Gamma(l-2ip+1)\Gamma(l+2ip+1)}{\Gamma(2ip-l)\Gamma(-l-2ip)} \\
&\times \frac{\Gamma(2ip)\Gamma(-l-2ip) - \mathcal{R}\Gamma(-2ip)\Gamma(2ip-l)}{\Gamma(2ip)\Gamma(l-2ip+1) - \mathcal{R}\Gamma(-2ip)\Gamma(l+2ip+1)} \\
&= \frac{[2k(r_+ - r_-)]^{2l+1}\Gamma(l)\Gamma(l+1)(\Gamma(2l+n+2))}{\Gamma(2l)\Gamma(2l+1)\Gamma(2l+2)^2\Gamma(n+1)} \\
&\times 2ip \prod_{j=1}^l (j^2 + 4p^2) \frac{1 - \mathcal{R} \prod_{j=1}^l \frac{j-2ip}{j+2ip}}{1 + \mathcal{R} \prod_{j=1}^l \frac{j-2ip}{j+2ip}}. \tag{B46}
\end{aligned}$$

-
- [1] A. Berlin, N. Blinov, G. Krnjaic, P. Schuster, and N. Toro, Phys. Rev. D **99**, 075001 (2019), 1807.01730.
- [2] A. Arvanitaki, S. Dimopoulos, S. Dubovsky, N. Kaloper, and J. March-Russell, Phys. Rev. D **81**, 123530 (2010), 0905.4720.
- [3] I. G. Irastorza and J. Redondo, Prog. Part. Nucl. Phys. **102**, 89 (2018), 1801.08127.
- [4] G. Arcadi, M. Dutra, P. Ghosh, M. Lindner, Y. Mambrini, M. Pierre, S. Profumo, and F. S. Queiroz, Eur. Phys. J. C **78**, 203 (2018), 1703.07364.
- [5] M. Schumann, J. Phys. G **46**, 103003 (2019), 1903.03026.
- [6] J. M. Gaskins, Contemp. Phys. **57**, 496 (2016), 1604.00014.
- [7] D. Baumann, H. S. Chia, J. Stout, and L. ter Haar, JCAP **12**, 006 (2019), 1908.10370.
- [8] S. Detweiler, Phys. Rev. D **22**, 2323 (1980), URL <https://link.aps.org/doi/10.1103/PhysRevD.22.2323>.
- [9] A. A. Starobinskii, Journal of Experimental and Theoretical Physics (1973), URL <https://api.semanticscholar.org/CorpusID:2923717>.
- [10] R. Brito, V. Cardoso, and P. Pani, Lect. Notes Phys. **906**, pp.1 (2015), 1501.06570.
- [11] O. J. C. Dias, G. Lingetti, P. Pani, and J. E. Santos, Phys. Rev. D **108**, L041502 (2023), 2304.01265.
- [12] P. Pani, V. Cardoso, L. Gualtieri, E. Berti, and A. Ishibashi, Phys. Rev. D **86**, 104017 (2012), URL <https://link.aps.org/doi/10.1103/PhysRevD.86.104017>.
- [13] D. Baumann, H. S. Chia, R. A. Porto, and J. Stout, Phys. Rev. D **101**, 083019 (2020), 1912.04932.
- [14] S. S. Bohra, S. Sarkar, and A. A. Sen (2023), 2312.07295.
- [15] R. Brito, V. Cardoso, and P. Pani, Class. Quant. Grav. **32**, 134001 (2015), 1411.0686.
- [16] R. Brito, S. Ghosh, E. Barausse, E. Berti, V. Cardoso, I. Dvorkin, A. Klein, and P. Pani, Phys. Rev. Lett. **119**, 131101 (2017), 1706.05097.

- [17] A. Arvanitaki, M. Baryakhtar, S. Dimopoulos, S. Dubovsky, and R. Lasenby, Phys. Rev. D **95**, 043001 (2017), URL <https://link.aps.org/doi/10.1103/PhysRevD.95.043001>.
- [18] L. Tsukada, T. Callister, A. Matas, and P. Meyers, Phys. Rev. D **99**, 103015 (2019), 1812.09622.
- [19] J. Zhang and H. Yang, Phys. Rev. D **101**, 043020 (2020), 1907.13582.
- [20] S. J. Zhu, M. Baryakhtar, M. A. Papa, D. Tsuna, N. Kawanaka, and H.-B. Eggenstein, Phys. Rev. D **102**, 063020 (2020), 2003.03359.
- [21] S. Sun and Y.-L. Zhang, Phys. Rev. D **104**, 103009 (2021), 2003.10527.
- [22] L. Tsukada, R. Brito, W. E. East, and N. Siemonsen, Phys. Rev. D **103**, 083005 (2021), 2011.06995.
- [23] J. Yang, N. Xie, and F. P. Huang (2023), 2306.17113.
- [24] J. a. L. Rosa, J. P. S. Lemos, and F. S. N. Lobo, Phys. Rev. D **101**, 044055 (2020), 2003.00090.
- [25] A. Almheiri, D. Marolf, J. Polchinski, and J. Sully, JHEP **02**, 062 (2013), 1207.3123.
- [26] J. Polchinski, in *Theoretical Advanced Study Institute in Elementary Particle Physics: New Frontiers in Fields and Strings* (2017), pp. 353–397, 1609.04036.
- [27] P. O. Mazur and E. Mottola, Universe **9** (2023), ISSN 2218-1997, URL <https://www.mdpi.com/2218-1997/9/2/88>.
- [28] F. E. Schunck and E. W. Mielke, Class. Quant. Grav. **20**, R301 (2003), 0801.0307.
- [29] K. Skenderis and M. Taylor, Phys. Rept. **467**, 117 (2008), 0804.0552.
- [30] I. Agullo, V. Cardoso, A. D. Rio, M. Maggiore, and J. Pullin, Phys. Rev. Lett. **126**, 041302 (2021), 2007.13761.
- [31] J. D. Bekenstein and V. F. Mukhanov, Phys. Lett. B **360**, 7 (1995), gr-qc/9505012.
- [32] C. Rovelli and L. Smolin, Nucl. Phys. B **442**, 593 (1995), [Erratum: Nucl.Phys.B 456, 753–754 (1995)], gr-qc/9411005.
- [33] C. Rovelli, Phys. Rev. Lett. **77**, 3288 (1996), gr-qc/9603063.
- [34] A. Ashtekar, J. Baez, A. Corichi, and K. Krasnov, Phys. Rev. Lett. **80**, 904 (1998), gr-qc/9710007.
- [35] A. Ashtekar, J. C. Baez, and K. Krasnov, Adv. Theor. Math. Phys. **4**, 1 (2000), gr-qc/0005126.
- [36] I. Agullo, J. F. Barbero G., J. Diaz-Polo, E. Fernandez-Borja, and E. J. S. Villasenor, Phys. Rev. Lett. **100**, 211301 (2008), 0802.4077.
- [37] I. Agullo, J. Fernando Barbero, E. F. Borja, J. Diaz-Polo, and E. J. S. Villasenor, Phys. Rev. D **82**, 084029 (2010), 1101.3660.
- [38] G. J. Fernando Barbero, J. Lewandowski, and E. J. S. Villasenor, Phys. Rev. D **80**, 044016 (2009), 0905.3465.
- [39] S. A. Teukolsky, Phys. Rev. Lett. **29**, 1114 (1972), URL <https://link.aps.org/doi/10.1103/PhysRevLett.29.1114>.
- [40] S. A. Teukolsky, Astrophys. J. **185**, 635 (1973).
- [41] J. D. Bekenstein, Phys. Rev. D **7**, 2333 (1973), URL <https://link.aps.org/doi/10.1103/PhysRevD.7.2333>.
- [42] D. Christodoulou, Phys. Rev. Lett. **25**, 1596 (1970), URL <https://link.aps.org/doi/10.1103/>

- [PhysRevLett.25.1596](#).
- [43] S. W. Hawking, Phys. Rev. Lett. **26**, 1344 (1971), URL <https://link.aps.org/doi/10.1103/PhysRevLett.26.1344>.
 - [44] S. Hod, Phys. Rev. Lett. **81**, 4293 (1998), gr-qc/9812002.
 - [45] A. Coates, S. H. Völkel, and K. D. Kokkotas, Phys. Rev. Lett. **123**, 171104 (2019), 1909.01254.
 - [46] S. Datta and K. S. Phukon, Phys. Rev. D **104**, 124062 (2021), 2105.11140.
 - [47] R.-Z. Guo, C. Yuan, and Q.-G. Huang, Phys. Rev. D **105**, 064029 (2022), 2109.03376.
 - [48] V. Cardoso, M. Cavaglia, and L. Gualtieri, JHEP **02**, 021 (2006), hep-th/0512116.
 - [49] J. a. G. Rosa and T. W. Kephart, Phys. Rev. Lett. **120**, 231102 (2018), 1709.06581.
 - [50] L. Chen, D. Huang, and C.-Q. Geng (2023), 2311.01819.
 - [51] R.-Z. Guo, C. Yuan, and Q.-G. Huang, JCAP **04**, 069 (2023), 2301.06840.
 - [52] Y. Cao and Y. Tang, Phys. Rev. D **108**, 123017 (2023), 2307.05181.
 - [53] V. Cardoso, T. Igata, A. Ishibashi, and K. Ueda, Phys. Rev. D **100**, 044013 (2019), 1904.05109.
 - [54] N. Jia, Y.-D. Guo, G.-R. Liang, Z.-F. Mai, and X. Zhang (2023), 2309.05108.
 - [55] E. Berti, V. Cardoso, and A. O. Starinets, Class. Quant. Grav. **26**, 163001 (2009), 0905.2975.
 - [56] T. M. MacRobert, Nature **175**, 317 (1955), URL <https://api.semanticscholar.org/CorpusID:21329182>.